JOURNAL OF CATALYSIS **158,** 13–22 (1996)
ARTICLE NO. 0002

Peculiarities of Nickel Oxide Structure Transformation upon CO Hydrogenation

II. Dynamics of Phase Transformation

O. S. Morozova,*,[1] G. N. Kryukova,† D. P. Shashkin,* L. M. Plyasova,† and O. V. Krylov*

*Semenov Institute of Chemical Physics of Russian Academy of Sciences, ul. Kosygina 4, Moscow 117334, Russia; and
†Boreskov Institute of Catalysis of Siberian Branch of Russian Academy of Sciences, prospekt Lavrentieva 5, Novosibirsk 630090, Russia

Received January 24, 1994; revised August 15, 1995

The effect of initial microstructure and morphology of the NiO precursor on morphological peculiarities and catalytic properties of the multiphase catalysts for the CO hydrogenation was studied using *in situ* X-ray powder diffraction and transmission electron microscopy. Under the CO hydrogenation conditions, the NiO sample with the most developed (100) plane was found to be transformed into the $Ni/Ni_3C/NiO$ catalyst, giving CH_4 as a major product of the reaction. The NiO sample with the most developed (111) plane was transformed into the catalyst containing Ni_3C/NiO and producing equal amounts of CH_4 and CO_2. The catalytic properties of the samples were shown to be interrelated to both the composition of the multiphase catalyst and the morphology of each of the component. A step-by-step comparison between variations in the phase composition and the catalytic activity of the samples during a long-term treatment under the reaction conditions was carried out.

INTRODUCTION

Oxides of transition metals are commonly used as the precursors of the catalysts for the reaction of CO hydrogenation. Active catalysts containing the metal, carbide, and oxide phases are formed upon the treatment in the reaction mixture (1–5). The phase composition, as well as the catalytic activity of the sample, change during the treatment or under the reaction conditions. In the previous reports (2–4), we demonstrated the effect of the initial microstructure and morphology of NiO and α-Fe_2O_3 on the regularity of the solid-phase transformation and morphological peculiarities of the newly formed catalysts. In this work with the use of *in situ* X-ray diffraction (XRD) technique, we carried out a step-by-step comparison between the variations in the phase composition and the catalytic activity of the samples during a long-term treatment under the CO hydrogenation conditions.

The aim of our study is to find the correlation between the catalytic activity and the phase composition of Ni-containing catalyst. The major interest involves the effect of initial microstructure and morphology of NiO on the morphological peculiarities and catalytic activity of the multiphase catalyst. Transmission electron microscopy (TEM) was used for studying the morphology of the samples.

EXPERIMENTAL

Two samples of NiO, whose properties were described in detail previously (2), were utilized as precursors. Table 1 summarizes the properties of these oxides.

All the experiments were carried out at atmospheric pressure using a reaction mixture containing CO and H_2 in the ratio of $CO:H_2 = 1:1.5$ with an overall flow rate of 6 ml min^{-1} at the temperatures of 240–285°C. As a rule, the CO conversion did not exceed 10–12%.

Reactor

The flow reactor cell used in the simultaneous catalytic and XRD tests was similar to that employed in the previous studies (3, 7). The reactor was a 0.48-ml-vol stainless-steel chamber housed in an electric furnace and combined on-line with a gas chromatograph. Temperature was measured by using a chromel–alumel thermocouple located inside the reactor cell so that the temperature of the sample was registered. The gradientless conditions of the experiment were found before monitoring the catalytic and structural properties.

Experimental Procedure

The experiments were carried out according to the following procedure:

[1] To whom correspondence should be addressed.

0021-9517/96 $12.00

TABLE 1

Description of Nickel Oxide Samples

Sample	Preparation	Morphological peculiarity	Specific surface area ($m^2\ g^{-1}$)
NiO(I)	Plasmochemical method (6)	Cubic microcrystals with (100) developed planes. Mean particle size is equal to 40 nm, whereas larger crystals (over 200 nm) also exist.	20
NiO(II)	Air calcination of $NiCO_3$ (Merk) at 700°C for 5 h	Platelets with (111) developed planes and surface steps on lateral sides. Mean particle size is equal to 150 nm.	4.9

(i) The unreduced precursor NiO (ca. 0.4 g) was placed into the reactor cell and heated in a flow of He up to the initial temperature of the run.

(ii) At the given temperature, He was replaced by the reaction mixture. In order to ensure steady-state conditions in both the catalytic reaction and the structural transformations, the CO hydrogenation was performed during a period of about 90 or 300 min, as dictated by the sample and temperature of the run. When the steady-state conditions were achieved, the temperature was quickly (about 1 min) raised by 15°C. Thereafter, the experiment continued at the next temperature. A composition of the reaction mixture on the outlet of reactor and the phase composition of the sample were tested simultaneously every 10 min. Each of the analyses took ~10 min.

(iii) The XRD measurements indicated some amount of Ni_3C accumulated in the sample during the catalytic reaction (Figs. 1a and 4a). To estimate the content of Ni_3C, we used the reaction

$$Ni_3C + 2H_2 \rightarrow CH_4 + 3Ni, \qquad [1]$$

by which Ni_3C was transformed into CH_4 and Ni quantitatively. The reaction was carried out in the flow of mixture containing 5% H_2 in He. When the steady-state conditions were achieved, this mixture replaced reaction mixture. Under the treatment, the rate of CH_4 formation increased, passed through the maximum, and then decreased, as the content of Ni_3C decreased (Fig. 3). The disappearance of the Ni_3C peak in the XRD pattern (Figs. 1b and 4b) indicated the completion of the reaction [1]. The integral intensity of the Ni_3C diffraction peak was correlated with the amount of Ni_3C. The latter was calculated through the content of CH_4 being formed in the period when the peak disappeared. Some carbon being accumulated in the sample could also be hydrogenated under the same conditions:

$$C + 2H_2 \rightarrow CH_4. \qquad [2]$$

On the basis of special calibrations and balance calculations, reactions [1] and [2] were separated. We showed that ~79.3% of CH_4 was produced by reaction [1].

(iiii) When the process of CH_4 formation was completed, the reaction mixture was again passed through the reactor, and the experiment continued as was described in (ii).

To study the kinetics of the phase transformation, we systematically recorded the XRD pattern containing the characteristic peaks of NiO, Ni, and Ni_3C (Figs. 1 and 4). A scan speed of 1°/min was used. A Be(110) peak was used as an internal standard. The phase composition of the catalyst was verified by the JSPDC data files. The relative concentrations of the different phases in the sample were calculated on the basis of integral intensities of the characteristic diffraction peaks. The amount of Ni was determined from the calibration curve obtained for the mixture of Ni and NiO containing 0.9–100 mol% of the metal.

TEM investigations of the catalyst were carried out on the different stages of transformation. A JEM-100 CX electron microscope with 0.3-nm resolution and accelerating potential of 100 kV was used. The samples were prepared from ethanol suspension and replaced into the copper grids covered by the amorphous carbon.

RESULTS

NiO(I) Sample

The treatment of the initial NiO(I) in the reaction mixture at 240°C resulted in the partial reduction to Ni after ~80 min of the induction period. When the phase of Ni was detected in XRD pattern, CH_4 was found in the effluent gas. It took about 125 min to obtain the system containing ~4 mol% Ni in NiO. The conversion of CO on the catalyst did not exceed 1%. The products of the CO

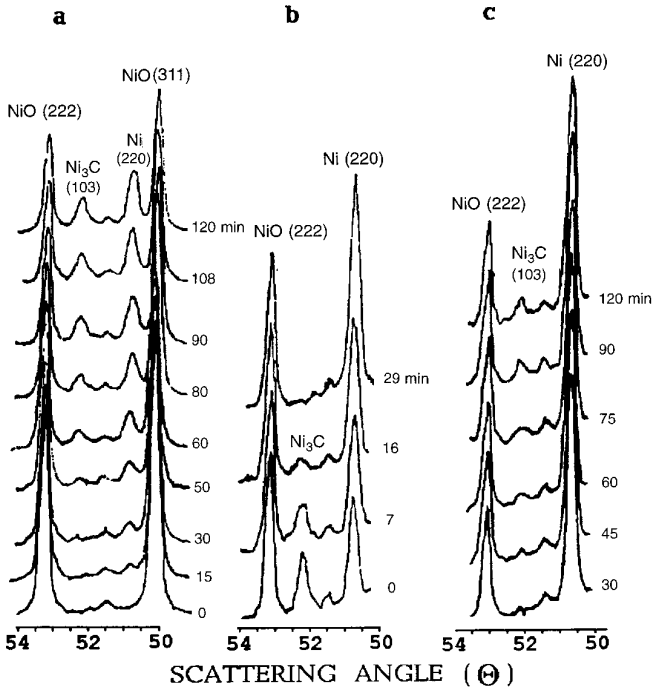

FIG. 1. *In situ* XRD spectra of NiO(I) obtained on Fe$K\alpha$ radiation during the CO hydrogenation at 255°C (a), during the treatment in a mixture containing 5% H_2 in He at 270°C (b), and during the CO hydrogenation at 270°C (c).

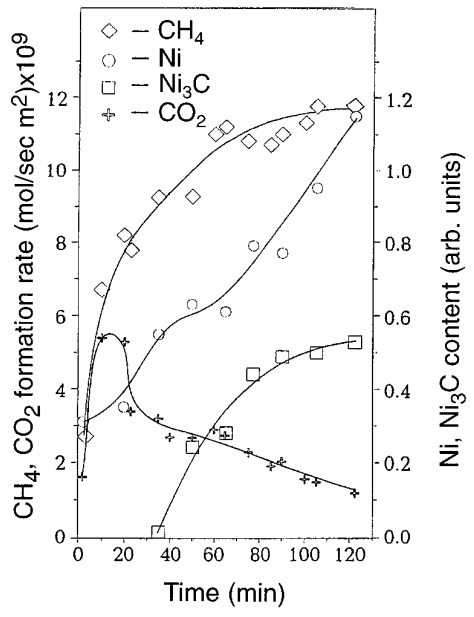

FIG. 2. Change in the integral intensities of Ni(220) and Ni_3C(103)—data from the on-line, time-resolved diffractograms in Fig. 1a—and variation in the rates of CH_4 and CO_2 formation obtained during the CO hydrogenation at 255°C.

hydrogenation consisted of CH_4 (30%) and CO_2(70%); water was not analyzed.

Figure 1a shows the XRD pattern obtained at 255°C under the reaction conditions. The (103) characteristic peak of Ni_3C at $\Theta = 52.17°$ was defined in the spectra after some induction period. The kinetic curves in Fig. 2 indicate that there were two pathways of NiO transformation: the reduction and carbidization processes took place simultaneously until the formation of Ni_3C was stabilized.

During the solid-phase transformations, the rate of CO_2 formation peaked in the first 10–12 min of the treatment and then decreased. The rate of CH_4 formation increased during the first 90 min of the run and then stabilized (1.13×10^{-8}–1.18×10^{-8} mol sec^{-1} m^{-2}), as well as the formation of Ni_3C. In Table 2 we relate directly the structural and catalytic properties of the sample at 255°C. On the basis of XRD measurements, we estimated the size of crystallites and specific surface area for the phase of NiO, Ni, and Ni_3C. The average size of the crystallites and the specific surface area of NiO were found to be ~44 nm and 20.6 m^2 g^{-1}, respectively. The average size of the Ni crystallites and the specific surface area were found to be ~40 nm and 20 m^2 g^{-1}, respectively. For Ni_3C, the average size of crystallites and the specific surface area were found to be ~33 nm and 16.1 m^2 g^{-1}, respectively. During the experiment, these values varied insignificantly. Thus, the specific surface area of the total sample remained virtually unchanged.

The calculation being made on the basis of crystallographic parameters of the unit cell, on average size of the particle, and specific surface area of the NiO(I) sample indicated that the phase transformations at 255°C touched the surface and subsurface layers of the oxide particles: from a layer of 1 unit cell thick to that of 3 unit cells thick.

At 270°C, the carbidization process renewed and reached the steady-state conditions in 60 min, when the reduction process evolved into the bulk of the oxide particles. At the end of the run, the reduction degree was found to be ~60 mol%. The calculations give the average depth of the NiO bulk conversion equal to 6 unit cells.

The rate of the carbidization reaction may fall and restart due to the broad variation in the size of the NiO(I) particles (from 20 to 200 nm). The reduction of the big crystals is slow, whereas a probability of Ni_3C formation is high. The reduction of the smaller microcrystals proceeds faster, so the carbidization of these particles is suppressed because the Ni layers form on the surface.

Following the solid-phase transformation, the rate of CH_4 stabilized in 60–70 min and later fluctuated in the range from 3.3×10^{-8} to 3.6×10^{-8} mol sec^{-1} m^{-2}. The rate of CO_2 formation decreased fivefold during the run. It seems to be the result of covering the whole particles of the catalyst by the metal, (100)Ni.

To compare the catalytic properties of the $Ni/Ni_3C/NiO$ and Ni/NiO samples, we treated the first one in a mixture

TABLE 2

Dynamics of NiO(I) Structural and Catalytic Properties on the First Cycle of Carbidization

T (°C)	t^a (min)	Conversion CO (%)	Selectivity^b (%)			Rate (mol sec^{-1} m^{-2})			Phase composition (mol%)		
						10^8	10^{10}	10^9			
			CH_4	C_2H_6	CO_2	CH_4	C_2H_6	CO_2	Ni	Ni_3C	NiO
255	30	3.5	70.7	4.6	24.4	0.77	3.3	3.3	7.0	—	93.0
	60	3.9	74.5	6.0	19.6	1.1	4.4	2.9	12.6	4.0	83.3
	90	4.3	79.9	5.9	14.2	1.13	4.2	2.1	17.0	7.4	75.4
	120	4.9	85.6	6.6	7.9	1.18	4.9	1.11	24.0	7.7	68.3
270	30	10.0	82.5	6.2	11.3	3.15	11.9	4.3	29.4	13.6	57.0
	60	9.7	85.4	7.0	7.5	3.2	13.2	2.8	34.3	17.8	47.9
	90	10.3	87.3	5.8	6.8	3.1	9.7	2.4	37.2	17.7	45.0
	120	10.0	87.7	8.1	4.2	3.5	16.5	1.65	40.5	18.3	41.0

[a] A time count from the beginning of the run.
[b] Product distribution is based on the content of CH_4, C_2H_6, and CO_2 detected continuously at every run.

containing 5% H_2 in He to remove Ni_3C. Figure 1b demonstrates the changes in XRD pattern of the catalyst during the treatment. The integral kinetic curves describing the solid-phase reaction and the CH_4 formation are shown in Fig. 3. After the treatment, the catalyst consisted of ~70 mol% Ni in NiO. The estimation on the basis of the mass balance indicated that $\sim 1 \times 10^{-3}$ g molecule^{-1} of Ni_3C and 3×10^{-4} g atom^{-1} of carbon were formed in the catalyst during the experiment.

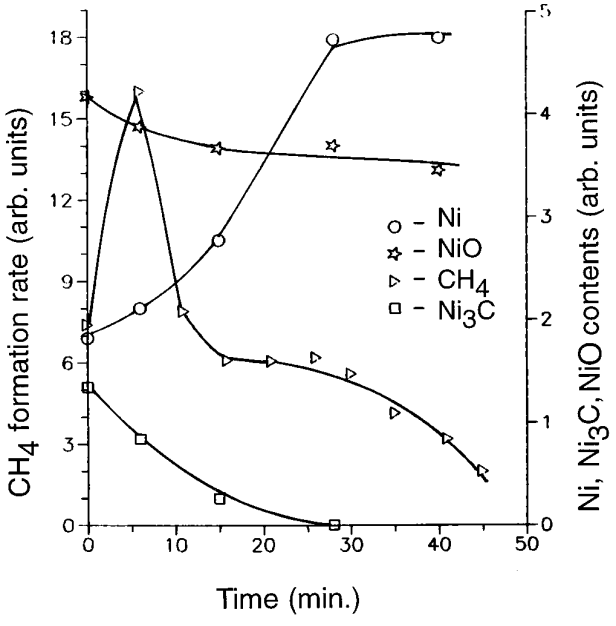

FIG. 3. Change in the integral intensities of NiO(200), Ni_3C(103), and NiO(222)—data from the on-line, time-resolved diffractograms in Fig. 1b—and variation in the rate of CH_4 formation obtained during the treatment in the mixture of 5% H_2/He at 270°C.

When the newly formed Ni/NiO catalyst was treated upon the reaction mixture, Ni_3C was detected after 30 min of the treatment at 270°C (Fig. 1c). The rate of carbidization at 270°C was lower than that observed at 255°C for the initial sample. According to TEM data, the layer of metallic nickel (100) was formed on the surface of NiO particles because of the orientation relationship $[100]_{Ni}/[100]_{NiO}$ (2). It seems that these layers suppressed partially the carbidization process. The relationship between the catalytic properties and the phase composition is exhibited in Table 3. At 255°C, the conversion of CO was found to be almost 2-fold higher, as compared to that for the Ni/Ni_3C/NiO catalyst (Table 2). The distribution of the products was also changed: the rate of C_2H_6 formation was found to be almost 10-fold higher and the rate of CO_2 formation was found to be almost 10-fold lower than these observed on the initial sample (Table 2). At the same time, the rates of CH_4 formation were of the same order of magnitude for the Ni/NiO and Ni/Ni_3C/NiO catalysts. However, the rates of CH_4 formation on the Ni/NiO catalyst were virtually constant from the beginning of the run. When the temperature increased to 270°C, the following changes in catalytic activity were observed: the conversion of CO, as well as the rates of CH_4 and CO_2 formation, increased and the rate of C_2H_6 formation lowered somewhat. The production of the Ni_3C phase was marked by the drastic increase of the rate of CO_2 formation. It was found to be almost 10-fold higher than that at 255°C in the absence of Ni_3C, while the rate of CH_4 increased by 1.5–2 times. The catalytic properties of the samples listed in Tables 2 and 3 became approximately the same at 270°C. All the parameters observed became virtually equal after the 120-min exposure under the reaction conditions in spite of the different bulk composition. This result points to the

TABLE 3

Dynamics of NiO(I) Structural and Catalytic Properties on the Second Cycle of Carbidization

T (°C)	t^a (min)	Conversion CO (%)	Selectivity^b (%)			Rate (mol sec^{-1} m^{-2})			Phase composition (mol%)		
						10^8	10^9	10^{10}			
			CH_4	C_2H_6	CO_2	CH_4	C_2H_6	CO_2	Ni	Ni_3C	NiO
255	30	8.1	79.8	18.3	1.9	1.9	2.2	4.5	75.0	—	25.0
	60	7.4	82.6	16.4	1.0	1.8	1.8	2.3	75.3	—	24.7
	90	6.8	78.7	20.5	0.4	1.5	2.0	0.8	76.4	—	23.5
	120	7.9	73.4	25.9	0.6	1.8	3.2	1.6			
270	30	11.9	85.6	10.2	4.2	3.4	2.0	16.7	76.3	Traces	23.6
	60	11.2	85.9	10.5	3.6	2.8	1.6	10.9	76.3	1.4	22.3
	90	11.0	86.5	9.9	3.6	3.2	2.0	14.2	75.2	2.3	22.5
	120	11.4	86.0	9.9	4.1	3.3	1.8	14.6	74.6	3.8	21.6

[a] A time count from the beginning of the run.
[b] Product distribution is based on the content of CH_4, C_2H_6, and CO_2 detected continuously at every run.

fact that the same surface conditions can be reached from both oxide and metal/oxide initial systems, as was reported in (1) for the iron catalyst.

NiO(II) Sample

The treatment of the initial NiO(II) sample under reaction conditions at 285°C resulted in nothing but Ni_3C formation, while the phase of Ni was not detected (Fig. 4a). The (201) and (112) diffraction peaks of Ni_3C were defined after 140 min of treatment. However, these peaks periodically appeared and disappeared on the diffractograms within 30–50 min from the beginning of the run. During the induction period, the lattice parameters of NiO increased. This is an indication of the insertion of carbon into the lattice of oxide. Table 4 summarizes results of the catalytic and XRD experiments. The initial catalytic activity was found within 20 min from the beginning of

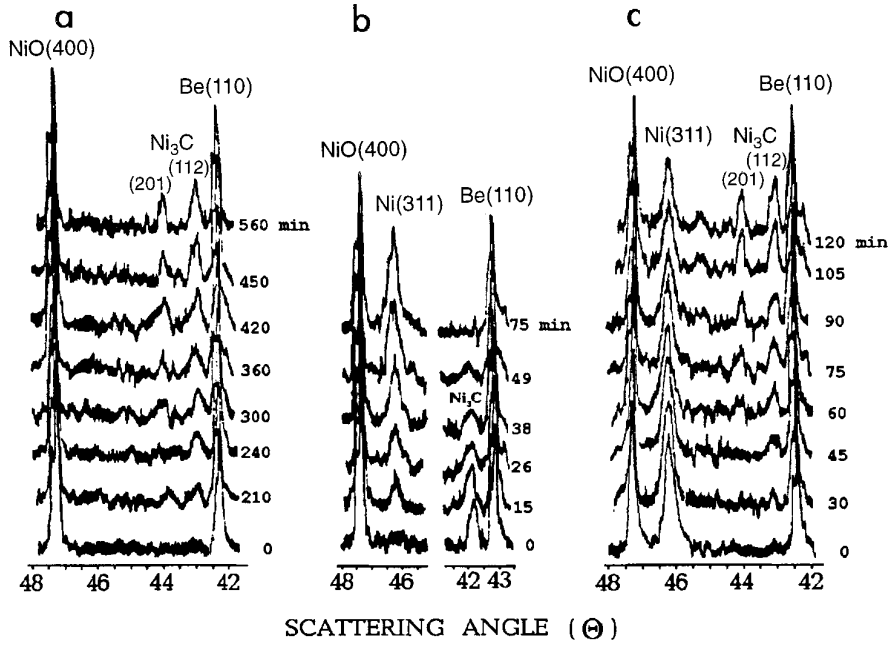

FIG. 4. *In situ* XRD specta of NiO(II) obtained on Cu$K\alpha$ radiation under the treatment at 285°C in the mixtures, as follows: CO/H_2 (a), 5% H_2/He (b), and CO/H_2 (c).

TABLE 4

Dynamics of NiO (11) Structural and Catalytic Properties on the First and Second Cycles of Carbidization at 285°C

t^a (min)	Conversion CO (%)	Selectivity^b (%)			Rate (mol sec^{-1} m^{-2})			Phase composition (mol%)		
					10^8	10^9	10^8			
		CH_4	C_2H_6	CO_2	CH_4	C_2H_6	CO_2	Ni	Ni_3C	NiO
					The first cycle					
A										
30	0.55	23.8	—	66.2	0.28	—	0.9	—	—	100
90	0.86	33.1	—	66.9	0.64	—	1.3	—	Traces	100
120	1.15	33.1	—	66.9	1.0	—	2.3	—	Traces	100
150	1.9	33.7	—	66.3	1.3	—	2.6	—	0.96	99.1
180	2.2	34.8	—	65.2	1.5	—	2.8	—	1.04	99.0
210	2.6	38.9	—	61.1	2.0	—	3.2	—	2.5	97.5
240	3.0	40.8	—	59.2	2.3	—	3.4	—	3.0	97.0
270	3.3	42.8	—	57.2	2.9	—	3.8	—	3.9	96.1
B										
30	4.6	39.7	—	60.3	3.5	—	5.3	—	3.9	96.1
60	5.4	43.2	—	56.8	4.5	—	6.0	—	4.0	96.0
90	6.5	45.8	—	54.2	5.5		6.5	—	4.6	95.3
120	7.5	45.3	3.3	51.4	6.6	2.1	7.5	—	4.8	95.2
150	8.4	46.2	3.6	50.2	7.4	2.9	8.1	—	—	—
180	8.3	45.8	3.5	50.6	7.3	2.8	8.0	—	5.0	95.0
210	8.7	48.1	4.0	47.9	8.1	3.4	8.0	—	5.1	94.9
240	9.0	48.4	4.4	47.2	8.4	3.8	8.2	—	5.4	94.6
270	9.7	47.6	4.4	48.0	7.9	3.6	7.9	—	5.1	94.9
					The Second Cycle					
30	8.5	48.8	8.3	42.9	8.1	1.7	7.1	16.0	0.98	82.9
60	9.7	44.2	5.4	50.3	8.1	5.9	9.3	15.5	2.6	81.9
90	10.9	44.8	4.5	50.6	10.1	5.0	11.5	12.9	3.8	83.2
105	13.3	44.8	4.6	50.6	12.0	6.2	13.5	11.6	6.2	82.2

Note. **A**, the first day under the treatment. **B**, the continuation of the treatment after 20 h; the catalyst was left at 20°C on the He flow.

[a] A time count from the beginning of the run.

[b] Product distribution is based on the content of CH_4, C_2H_6, and CO_2 detected continuously at every run.

the run, when the phase of Ni_3C was not observed. TEM data also evidenced for the absence of the Ni_3C particles in the NiO(II) sample on this activation stage. The conversion of CO and the rate of CH_4 formation were found to be very low in the first ~120 min of the run that indicate a small amount of the active sites on the surface. We have no data with which to discuss the nature of these sites. Nevertheless, the surface steps of the oxide microcrystal observed by TEM, inclusions of the active carbon, or the small amount of the high dispersed Ni_3C seems to be associated with these. When the phase of Ni_3C appeared, the conversion of CO, as well as the rates of CH_4 and CO_2, increased. Figure 5 exhibits a direct relationship between the content of Ni_3C and the parameters of the catalytic process. After ~480 min, when the catalyst contained ~5.1 mol% of Ni_3C, nearly steady-state conditions of both the catalytic and topochemical processes were reached.

In the next stage of the experiment, we obtained a Ni/NiO system through the treatment of the Ni_3C/NiO catalyst in the mixture of 5% H_2 in He at 285°C (Fig. 4b). According to XDR results, the system being prepared contained ~18 mol% of Ni. TEM data indicated the polycrystalline structure of the metal.

As shown in Fig. 4c, the Ni/NiO sample easily transformed into the multiphase catalyst Ni_3C/Ni/NiO under the reaction conditions. The catalytic and structural properties are summarized in Table 4. Figure 5 exhibits that a direct relationship between the content of Ni_3C and the rates of CH_4 and CO_2 formation is retained. In the presence of metallic Ni, the conversion of CO and the rates of CH_4 and CO_2 were found to be several times higher, as compared to those in the absence of the metal (Table 4). However, the difference between the properties observed was not so drastic, as in the case of the catalysts obtained from the sample NiO(I).

Both the CH_4 and C_2H_6 selectivity on the catalyst obtained from NiO(II) was found to be nearly twice as small as those on the catalyst obtained from NiO(I) because of the relatively high rate of CO_2 formation. According to the data listed in Tables 2–4, this rate was found to be

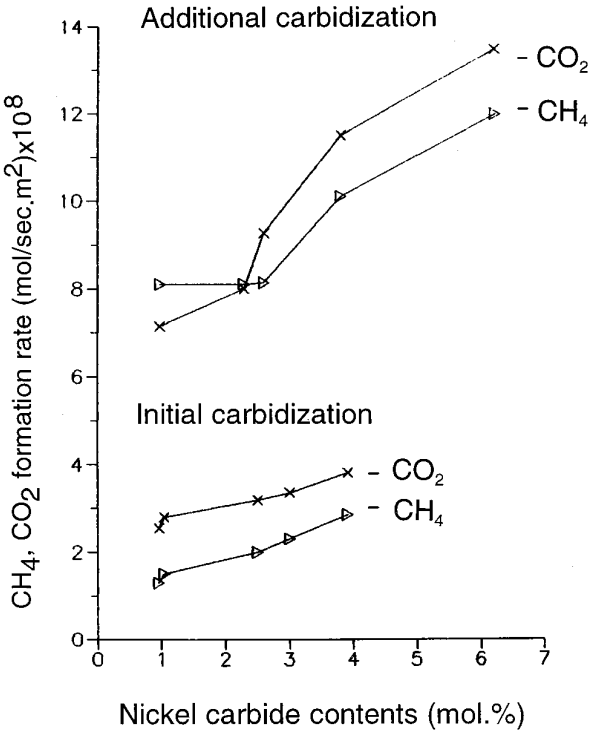

FIG. 5. The dependence between the content of Ni_3C and the rates of CH_4 and CO_2 formation on the initial (I) and the additional (II) carbidization stages.

more 10 to 100 times higher on Sample II than that on Sample I, whereas the rates of CH_4 and C_2H_6 were of the same order of magnitude for both of these samples. In contrast to Sample I, the formation of CO_2 was not suppressed in the presence of metallic Ni on Sample II (the second cycle of carbidization).

DISCUSSION

The careful examination of the experimental results led us to the following important conclusions: (i) the initial microstructure and morphology of NiO define the structure and the catalytic properties of the newly formed catalyst, and (ii) the solid-phase transformations and the catalytic reaction are interdependent ones because of the participation of CO and H_2 in both of the processes.

The effect of the initial microstructure of the NiO precursor on the catalytic properties can be easily realized through the interdependence between the topochemical and catalytic reactions.

Previously, we reported that even for the polycrystalline powder samples the mechanism of solid-phase transformation depends on the structural similarity between the crystal lattices of the reagent and the product (2). Thus, due to the structural similarity between cubic unit cells of NiO and Ni, a layer of the metal, (100)Ni, was first of all formed on the surface (100) of the NiO(I) sample under the treatment in the reaction mixture. Dufour *et al.* (8–10) indicated a leading role of atomic hydrogen in the reduction of the (100) plane of NiO. The point defects and Ni atoms with the low coordination number were found to be the centers of H_2 dissociation. These studies strongly suggest that the growth of the metallic phase passes through nucleation in the hexagonal structure near 250°C. At the higher temperatures, Ni nucleated in its usual face-centered cubic structure. The interface between NiO and the newborn Ni phase is constituted by the (111) planes, which correspond in both lattices and placed lengthwise on the (111) plane of NiO.

The interesting feature of the study was the observation that CO reacts with the (100) plane of NiO only in the presence of the hydrogen traces. No reduction was detected below 270°C in pure CO. Our studies (2) indicated the key role of CO in the topochemical process: the dissociative adsorption of CO resulted in the insertion and accumulation of carbon into the bulk of NiO accompanied by the destruction of NiO(I) particles. As a result, the multigraded NiO microcrystals were formed.

On the basis of the model for reduction of the (100) NiO proposed in (8), our XRD and TEM data reported in (2, 11, 12), and the aforementioned experimental results, we formulated the scheme for the solid-phase transformation of NiO(I) initiated by the interaction with the reagents (CO and H_2) (Fig. 6). Through this scheme, we attempted

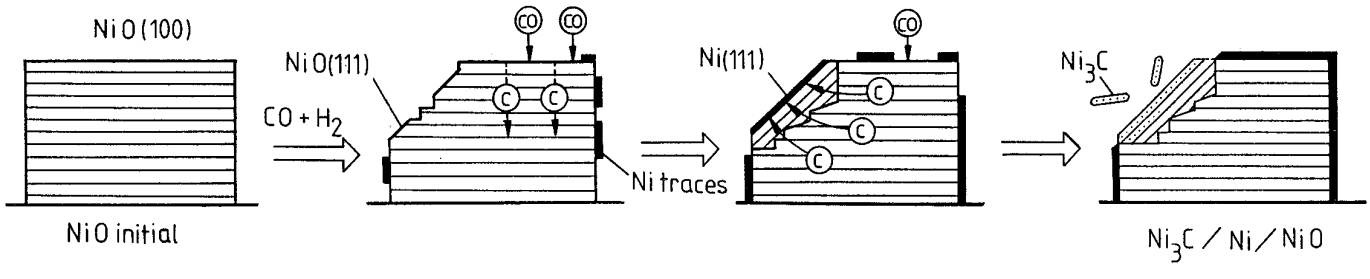

FIG. 6. A scheme for the solid-state transformation of NiO(I) under reaction conditions.

to illustrate the initial stages of the reduction–carbidization process and to correlate step-by-step the peculiarities of the topochemical and catalytic reactions.

According to (11), the concentration of point defects in cubic structure of the initial NiO(I) is high. Therefore, after the H_2 dissociation, the interaction of H_2 and CO with the oxide could proceed through the stages, as follows:

$$2H_2 + O_{lat} \rightarrow H_2O + V_{lat} \quad [3]$$

$$CO + O_{lat} \rightarrow CO_2 + V_{lat} \quad [4]$$

$$CO + V_{lat} \rightarrow C_{intrinsic} + O_{lat} \quad [5]$$

$$CO + Ni \rightarrow CO_{ads}Ni \quad [6]$$

$$CO_{ads} + CO_{ads} \rightarrow C_{intrinsic} + CO_2, \quad [7]$$

where O_{lat} and V_{lat} are the lattice oxygen and oxygen vacancy, respectively. The interaction of H_2 with the surface of NiO results in the formation of Ni atoms scattered on the oxide. These atomic species and the oxygen vacancies could be considered as adsorption sites for the CO molecules (10). Reduction of the surface [3, 4], as well as $C_{intrinsic}$ formation [5, 7], also take place. Atomic carbon being formed accumulates in the bulk of the oxide (2). It seems to localize on the metal-oxide interface or ''fall'' into the crystal volume with the formation of carbon clusters (2, 13–15). The fact that the NiO lattice parameters increase in the first stage of the treatment justifies our assumption. TEM also indicates the presence of the small carbon clusters in the subsurface layers of the NiO(I) microcrystals after the treatment at 240°C. As was shown by TEM (2), the destruction of the perfect microcrystals of NiO(I) into the stepped ones took place under the action of carbon clusters. The adsorption and activation of the CO and H_2 molecules, as well as the reduction of NiO, seem to proceed faster on the fresh surface of the steps. The activated molecules take place in both the reduction of NiO and formation of CH_4. Thus, the topochemical process is in competition with the catalytic one. When the treatment was carried out at 240°C, the conversion of CO was only a fraction of a percentage. As the phase of Ni appeared, methane was detected in the products of the reaction, but CO_2 was found to be the major one. Until Ni_3C was defined, the rate of CH_4 formation increased proportionally to the increase of the metal content. Conversion of CO also increased, whereas the rate of CO_2 decreased after peaking. This effect seems to be associated with the newborn active Ni-containing centers giving the portion of activated H_2 molecules sufficient for both of the processes: the continued reduction and the catalytic hydrogenation.

At 255°C, the phase of Ni_3C was obtained in the Ni/NiO catalyst. In general, the formation of Ni_3C on the (100) planes of NiO or Ni is almost impossible due to lack of orientation similarity between these planes and any of the planes of the Ni_3C hexagonal unit cell. Previously (2, 12), we reported that the orientation similarity between the parent and carbide phases is the necessary condition for the Ni_3C formation. Close inspection of the Ni/NiO system indicates that the interface between Ni and NiO could be the only plane for the Ni_3C formation. It is located lengthwise on the (111) plane of NiO, corresponds with the (111) plane of Ni, and has a crystallographic similarity with the [0001] base plane of Ni_3C (Fig. 6). The formation of Ni_3C requires only the stoichiometric amount of carbon atoms accumulated on the interface through the diffusion of $C_{intrinsic}$ (13). Indeed, the induction period of the carbidization reaction was actually observed (Fig. 2). When Ni_3C was defined in X-ray spectra for the first time, its content was in good agreement with the amount of carbon being accumulated in the catalyst during the experiment. The estimation was carried out assuming reaction [7] to be the major contributor of carbon. Figure 6 shows that the stepped surface of the NiO microcrystal is also suited for the formation of Ni_3C: according to TEM data, the steps are placed lengthwise to the (111) plane of NiO and closely related to (111) plane of Ni.

When the phase of Ni_3C appeared, the rate of CH_4 increased proportionally to its content until steady-state conditions were achieved. On the basis of TEM data, we suppose that steady-state conditions correspond to the microcrystals of NiO(I) covered by the metal, (100)Ni. On this kind of sample, the formation of Ni_3C is suppressed because the (100) plane of Ni is devoid of an orientation similarity with the Ni_3C planes, and the rate of CH_4 formation stabilizes. On the basis of these data, it is conceivable that two types of the centers for the CH_4 formation are presented on the surface. Under steady-state conditions, the major part of the centers seems to be located on the (100)Ni surface because the rate of CH_4 formation is independent of the reduction degree. Otherwise, when both reduction and carbidization processes take place, the most active centers could be located on the interfaces between the newly formed phases. The unusual hexagonal nuclei of Ni were found to be formed on the interface (100)NiO/Ni (10). Under the non-steady-state conditions, these nuclei or other unstable but active centers located on the interface can be responsible for part of the CH_4 formation. Until the interface Ni/Ni_3C/NiO is accessible to the reagents, the rate of CH_4 formation is proportional to the Ni_3C content, which is placed on this interface.

The solid-phase transformation of the NiO(II) sample under the reaction conditions was described in the previous report (2). Because of the crystallographic similarity between the (111) plane of the initial NiO(II) and the [0001] base plane of hexagonal crystal lattice Ni_3C, only the phase of Ni_3C was formed. According to TEM results, forming Ni_3C microcrystals were placed on the surface of the oxide, as similar-sized platelets. Then, the Ni_3C platelets lose con-

tact with the ''parent'' NiO particle followed by the formation of the new Ni_3C microcrystals.

In spite of the simplicity of the structural transformation of NiO(II), the process began at a higher temperature and after a longer induction period as compared to Sample I. This seems to be associated with two factors: (i) the difficulties in removing oxygen from the (111) plane of NiO and (ii) the accumulation of the definite amount of $C_{intrinsic}$ in the subsurface layer of the oxide microcrystal.

According to TEM results (11), concentration of point defects in this sample is low; therefore activation of H_2 and CO takes place only on the surface steps of the NiO(II) microcrystals. The concentration of such centers does not seem to be high. Thus, the removal of oxygen from the surface of oxide, as well as the accumulation of carbon, is a slow process. The most likely speculation about the catalyst state is that the partially reduced surface of the (111) plane of NiO is promoted with carbon. According to (15, 16), the rate of dissociative adsorption of H_2 on this kind of surface is low, as compared to that of Sample I. However, the carbon clusters with a negative charge may be considered the additional centers of CO adsorption (17).

Under non-steady-state conditions, the major portion of CO_2 was produced by reactions [4] and [7]. It seems that Ni_3C, part of CO_2, and CH_4 were formed from $C_{intrinsic}$, as follows:

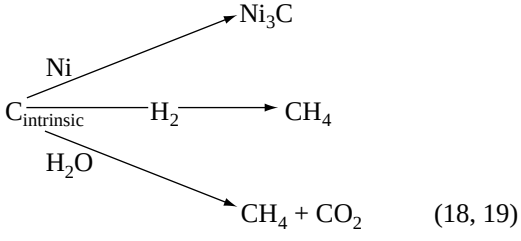

(18, 19)

As for the water–gas shift reaction, as a contributor of CO_2, the Ni-containing catalyst does not seem to be good for it.

We recall that both the rates of CO_2 and CH_4 formation increased, as the content of Ni_3C increased. Under the non-steady-state conditions, the rate of CO_2 exceeded the rate of CH_4. Under steady-state conditions, these rates were found to be almost equal. The CH_4 formation took place with the formal stoichiometry, as follows:

$$2CO + 2H_2 \rightarrow CH_4 + CO_2. \qquad [8]$$

When the Ni_3C/NiO catalyst was transformed into the Ni/NiO catalyst, the polycrystalline metal did not form a continuous layer on the surface of NiO(II) due to the absence of the structural similarity between the (111) plane of NiO and the cubic unit cell of Ni. Thus, the surface of oxide was still accessible for the reagents, and formation of Ni_3C was restarted immediately under the reaction conditions. In the presence of the metal, the rate of CH_4 increased in the beginning of the run, as compared to the rate of CO_2 (Fig. 5). However, when Ni_3C appeared, the ratio between the rates of CO_2 and CH_4 formation was found to be as before.

Thus, there is some evidence that CO activation may take place on the surfaces of the oxide, carbide, and metal, as well as on carbon inclusions. The carbon inclusions seem to be used for Ni_3C and CO_2 formation. Therefore, the interface between Ni_3C and NiO was highly profitable for CO_2.

The surface of the metal, especially (100) Ni, or the Ni clusters located on the surfaces of oxide or carbide phases seem to be suitable for H_2 activation. According to the data obtained for Sample II, the CO_2 formation was competitive with the CO hydrogenation when the centers for the H_2 activation were deficient. The catalyst with a high content of the metal, especially (100) Ni, was better suited for the methane formation. In none of the special prolonged experiments with the fine nickel powder as a catalyst (average size of the particles of 35 nm) (20), the deposition of coke or Ni_3C was observed. This phenomenon is associated with the high concentration of H atoms on the surface and in the bulk of the catalyst. The concentration could be enough for the hydrogenation of different forms of CO adsorbed hindering the carbon and Ni_3C production.

SUMMARY

The initial microstructure and morphology of the polycrystalline NiO precursor define the phase composition and the catalytic properties of the multiphase catalysts obtained for the CO hydrogenation. Under the treatment in the reaction mixture, the precursor with the (100) most developed plane was transformed into the Ni/Ni_3C/NiO catalyst containing the cubic microcrystals of NiO covered by the layer of (100)Ni and polycrystalline Ni_3C. The major product of reaction was found to be CH_4. Under similar conditions, the precursor with the (111) most developed plane was transformed into the Ni_3C/NiO catalyst involving the NiO platelets covered by ''monocrystals'' of Ni_3C and separate particles of Ni_3C. On this catalyst, CH_4 and CO_2 were formed to the same extent. The catalytic properties were found to be interrelated with the phase composition of the sample, as well as with the morphology of each of the phases.

ACKNOWLEDGMENT

The authors are thankful to Prof. A.Ya. Rozovskii (Moscow Institute of Petrochemical Synthesis) for valuable comments and discussion.

REFERENCES

1. Reymond, J. P., Meriandeau, P., and Teichner, S. J., *J. Catal.* **75,** 39 (1982).

2. Morozova, O. S., Ziborov, A. V., Kryukova, G. N., and Plyasova, L. M., *J. Catal.* **144,** 50 (1993).
3. Morozova, O. S., Maksimov, Yu. V., Shashkin, D. P., Shirjaev, P. A., Matveev, V. V., Zhorin, V. A., Krylov, O. V., and Kryukova, G. N., *Appl. Catal.* **78,** 227 (1991).
4. Morozova, O. S., Parshina, T. M., Sacharov, M. M., Maksimov, Yu. V., and Krylov, O. V., *in* "Proceedings, 4th All Union Conf. on the Mechanism of Catalytic Reactions, Moscow," Vol. I, pp. 375–379, 1986. [In Russian]
5. Heon Jung, and Thomson, W. J., *J. Catal.* **139,** 375 (1993).
6. Parkhomenko, V., and Tsybulev, P. N., *in* "Proceedings, 8th International Symposium on Plasmochemistry, Tokyo," Vol. 4, pp. 2105–2110, 1987.
7. Shirjaev, P. A., Kushnerev, M. Ya, Shashkin, D. P., and Krylov, O. V., *Kinet. Katal.* **23,** 1280 (1982).
8. Dufour, L.-C., Floquet, N., and De Rosa, B, *in* "Reactivity of Solids," Mat. Sci. Monograph 28 A, p. 47. Elsevier, Amsterdam, 1985.
9. Dufour, L.-C., and Perdereau, M., *in* "Surface and Near-Surface Chemistry of Oxide Materials" (J. Nowotny and L.-C. Dufour, Eds.), p. 577. Elsevier, Amsterdam, 1988.
10. Boudriss, A., and Dufour, L.-C., *in* "Non-stoichiometric Compounds, Surfaces, Grain Boundaries, and Structural Defects" (J. Nowotny and W. Weppner, Eds.), p. 311. Kluwer Academic, London/New York 1989.
11. Kryukova, G. N., Ph.D. thesis, Moscow, 1989.
12. Morozova, O. S., Ziborov, A. V., Kryukova, G. N., and Plyasova, L. M., *J. Solid State Chem.* **101,** 353 (1992).
13. Darling, G. R., Pendry, J. B., and Joyner, R. W., *Surf. Sci.* **221,** 69 (1989).
14. Zonnevylle, M. C., Geerlings, J. J., and van Santen, R. A., *Surf. Sci.* **240,** 253 (1990).
15. Benziger, J. B., and Madix, R. J., *Surf. Sci.* **115,** 279 (1982).
16. Allen, W. M., Jones, W. E., and Pacey, P. D., *Surf. Sci.* **220,** 193 (1989).
17. Papageno, L., Conti, M., Caputi, L. S., *et al., Surf. Sci.* **219,** L565 (1989).
18. Fan, C.-Z., and Teng, X.-B., *J. Catal.* (*China*) **11,** 51 (1990).
19. Somorjai, G. A., *Catal. Rev.* **29,** 181 (1983).
20. Petrov, Yu. I., *in* "Clusters and Small Molecules," p. 11. Nauka, Moscow, 1988. [In Russian]